Steel and Composite Structures, *Vol. 19, No. 5 (2015) 1299-1319*
DOI: http://dx.doi.org/10.12989/scs.2015.19.5.1299

Parametric study on eccentrically-loaded partially encased composite columns under major axis bending

Mahbuba Begum [1a], Robert G. Driver [*2] and Alaa E. Elwi [2b]

[1] *Department of Civil Engineering, BUET, Dhaka, Bangladesh*
[2] *Department of Civil and Environmental Engineering, University of Alberta, Edmonton, AB, Canada*

(*Received January 08, 2014, Revised January 15, 2015, Accepted May 20, 2015*)

Abstract. This paper presents a detailed parametric study, conducted using finite element tools to cover a range of several geometric and material parameters, on the behaviour of thin-walled partially encased composite (PEC) columns. The PEC columns studied herein are composed of thin-walled built-up H-shaped steel sections with concrete infill cast between the flanges. Transverse links are provided between the opposing flanges to improve resistance to local buckling. The parametric study is confined to eccentrically-loaded columns subjected to major axis bending only. The parameters that were varied include the overall column slenderness ratio (L/d), load eccentricity ratio (e/d), link spacing-to-depth ratio (s/d), flange plate slenderness ratio (b/t) and concrete compressive strength (f_{cu}). The overall column slenderness ratio was chosen to be the primary variable with values of 5, 10 and 15. Other parameters were varied within each case of L/d ratio. The effects of the selected parameters on the behaviour of PEC columns were studied with respect to the failure mode, peak axial load, axial load versus average axial strain response, axial load versus lateral displacement response, moment versus lateral displacement behaviour and the axial load–moment interaction diagram. The results of the parametric study are presented in the paper and the influences of each of the parameters investigated are discussed.

Keywords: composite; column; finite element; local buckling; partially encased; plate; slenderness ratio

1. Introduction

A partially encased composite (PEC) column section refers to an H–shaped steel section with concrete infill between the flanges, as shown in Fig. 1. In Europe, in the early 1980s, PEC columns and beams were introduced using standard-sized rolled wide-flange steel sections. In 1996, the Canam Group in North America proposed a PEC column section constructed from a thin–walled built–up steel shape with transverse links provided at regular intervals to restrain local buckling (Fig. 1). Using a built–up steel section instead of a standard shape provides the designer with more flexibility when sizing the column cross-section. Moreover, thin steel plates were specified to

∗Corresponding author, Professor, E-mail: rdriver@ualberta.ca
[a] Professor, E-mail: mahbuba@ce.buet.ac.bd
[b] Professor Emeritus, E-mail: aelwi@ualberta.ca

http://www.techno-press.org/?journal=scs&subpage=8 ISSN: 1229-9367 (Print), 1598-6233 (Online)

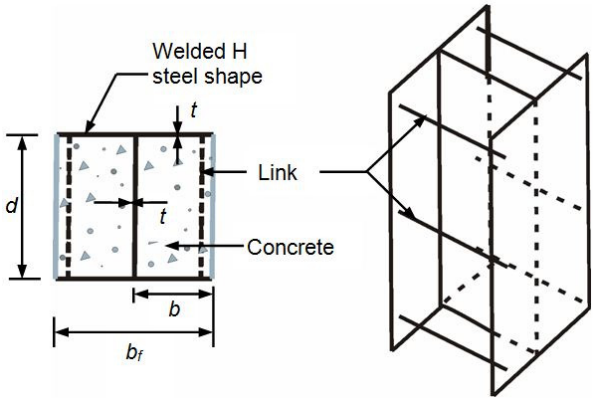

Fig. 1 Partially encased composite column with thin-walled built-up steel section: (a) column cross-section; and (b) 3d view of the steel configuration

obtain a more cost-effective column by increasing the contribution of concrete to its load carrying capacity. Also, for steel-framed high-rise structures, the thin-walled sections tend to reduce crane capacity requirements, which are often dictated by the weight of lower-storey steel columns. These factors have the potential to make PEC columns constructed with built-up shapes more attractive than those constructed with standard sections.

Most of the research on partially encased composite (PEC) columns (Tremblay *et al*. 1998, Chicoine *et al*. 2002, 2003, Zhao and Feng 2012) investigated concentrically-loaded applications; i.e., they were intended for use as "gravity" columns. However, the range of application of these columns can be expanded significantly by incorporating them as part of lateral load resisting systems such as braced frames or steel plate shear walls. To this end, Bouchereau and Toupin (2003), Pricket and Driver (2006) and Chen *et al*. (2010), tested PEC columns under combined axial load with monotonic and cyclic bending. Prickett and Driver (2006) also investigated the effects of high performance concrete on the behaviour of PEC columns. The results of these experimental investigations indicated that the behaviour and strength of this composite column is significantly affected by the initial local buckling of the thin steel flanges. Unlike fully encased composite columns (Uy 2001), the post-buckling strength is found to have negligible effects on the behaviour of this new composite column (Tremblay *et al*. 1998, Chicoine *et al*. 2002, 2003, Bouchereau and Toupin 2003, Pricket and Driver 2006 and Chen *et al*. 2010) Large-scale experimental investigations on steel plate shear walls with PEC columns were conducted by Deng *et al*. (2008) and Dastfan and Driver (2010a, b). As a part of a steel plate shear wall, the columns are subjected to the combined action of bending moment and axial force, and in some cases the moments can be substantial. Recent research on this new type of composite system includes its behaviour under thermal stresses conducted by Correia and Rodrigues (2011) and Young and Ellobody (2011). Design rules for PEC columns constructed with normal or high strength concrete and subjected to concentric gravity loading or combined axial load and bending have been incorporated into Canadian standard S16-09, *Design of Steel Structures* (CSA 2009).

The design procedure for PEC columns under combined axial load and bending have been validated mostly by tests on relatively short PEC columns, and there is a need for additional verification for columns with overall slenderness ratios, L/d, greater than 5. Experimental

investigations are, however, time consuming and capital-intensive, as well as being particularly challenging for long columns. Therefore, to investigate the behaviour of PEC columns constructed with both normal and high strength concrete subjected to axial compression and bending, a parametric analysis is required using a validated analytical model. Begum *et al*. (2007) developed a finite element modelling technique to predict the behaviour of this composite system under concentric or eccentric axial loading conditions. The model was applied successfully to reproduce the behaviour of 34 PEC columns from five experimental programs. The model was able to accurately trace a stable and complete load–strain history accurately for a variety of PEC columns with a wide range of geometric and material properties and under various loading conditions.

2. Objectives and scope

The primary objective of this research is to carry out a parametric study using finite element tools to explore the influences of geometric and material properties on the behaviour of PEC columns. As it has already undergone extensive validation exercises, the finite element model developed by Begum *et al*. (2007) is used.

The parametric study is confined to columns subjected to major axis bending only. The parameters that are varied include the overall column slenderness ratio (L/d), load eccentricity ratio (e/d), link spacing-to-depth ratio (s/d), plate slenderness ratio (b/t) and concrete compressive strength (f_{cu}). The overall column slenderness ratio was chosen to be the primary variable, with values of 5, 10 and 15 selected to cover a range from stocky to slender. Other parameters were varied within each case of L/d ratio.

3. Selected variable parameters

Overall column slenderness ratio (L/d)

Three different slenderness ratios—5, 10 and 15—were employed in the parametric study to cover the range of short, intermediate and slender columns. Thereby, this study will help to fill the gap in the behaviour of PEC columns resulting from the paucity of experimental data for columns with $L/d > 5$.

Initial load eccentricity ratio (e/d)

The load eccentricity ratios used in this study are 0.05, 0.15 and 0.30. The load eccentricity ratio of 0.05 is intended to represent an "accidental" eccentricity that might occur in a column that is nominally designed as a gravity column. The upper limit of 0.30 explores cases with substantial bending moments.

Flange plate slenderness ratio (b/t)

The flange plate slenderness ratio is defined as the ratio of the half-width of the flange, b, to its thickness, t. This parameter was varied between 25 and 35, with an intermediate value of 30. The ultimate capacity and failure mode of a PEC column is significantly affected by this parameter, since it controls the occurrence of local instability in the flange plate of the column.

Link spacing-to-depth ratio (s/d)

This parameter is defined as the ratio of link spacing, s, to the depth of the column cross-section, d. Two values of the s/d ratio—0.5 and 0.7—were used in the parametric study.

Link spacing is clearly an important parameter affecting the behaviour of these columns, since local buckling in the flange plates occurs between two successive links.

Compressive strength of concrete

In the parametric study, the concrete strength was varied from 30 MPa to 60 MPa to investigate the influence of high strength concrete in combination with other parameters.

4. Combinations of variable parameters

In designing the columns for the study, the overall column slenderness ratio, L/d, was considered the primary parameter. Other parameters were combined in an optimum and systematic way for each value of the primary parameter to obtain their individual effects and interrelationships. To facilitate this approach, three reference columns, designated "SN1", "IN1" and "LH1" (as shown in Table 1), are designed, where "S", "I" and "L" indicate short ($L/d = 5$), intermediate ($L/d = 10$) and long ($L/d = 15$) columns, respectively. To differentiate between the normal strength and high strength concrete columns, the letters "N" and "H" are included in the column designation. The number used in the column designation is simply a serial number. To study the effect of each selected parameter, numerical analyses were performed by varying only that parameter for each of the reference columns. In total, 31 columns were analysed for the parametric study, the details of which are given in Table 1.

5. Fixed geometric and material properties

All of the columns have a square cross-section with outer dimensions of 450 mm × 450 mm. This is a moderate size for composite columns and might be suitable in the construction of mid-rise buildings. The transverse links used were of 12.7 mm diameter, which meets the requirements of CSA S16-09 (CSA 2009). The parametric columns were assumed to be fabricated from CSA-G40.21 grade 350W steel plate. The nominal yield strength, F_y, of 350 MPa, the highest permitted by CSA S16-09 (CSA 2009) for PEC columns, was used in the analyses, and with an assumed modulus of elasticity of 200 GPa, the yield strain, ε_y, was taken as 0.00175 mm/mm. The ultimate strength of the steel plate is taken as 450 MPa and the corresponding strain is assumed to be 100 times the yield strain, i.e., 0.175 mm/mm.

Two types of concrete, with nominal strengths of 30 MPa and 60 MPa, were used in the parametric study. To define the concrete stress–strain curves for the finite element analyses of these columns, the strain corresponding to the uniaxial compressive strength, the elastic modulus and the Poisson's ratio are required. The strain at the ultimate compressive strength was calculated using the expression proposed by Almusallam and Alsayed (1995)

$$\varepsilon_{cu} = \left(0.2 f_{cu} + 13.06\right) \times 10^{-4} \tag{1}$$

which was developed based on experimental investigations of both normal and high strength concrete (up to 100 MPa). The elastic moduli for the normal and high strength concrete were calculated using the following expression according to ACI 363R-92 (ACI 1992)

$$E_c = 3320\sqrt{f_{cu}} + 6900 \tag{2}$$

In Eqs. (1) and (2), f_{cu} has units of MPa. The calculated values of elastic modulus and the strain at the ultimate compressive strength for concrete used in the parametric columns are listed in Table 1. The Poisson's ratio for concrete was taken as 0.20, as reported by Rashid *et al*. (2002) for concrete with strengths ranging from 20 to 120 MPa.

Table 1 Details of PEC columns for parametric study

Column designation	L/d	e/d	b/t	s/d	Global imperfection (mm)	f_{cu} (MPa)	ε_{cu} ($\mu\varepsilon$)	E_c (MPa)
SN1[(a)]	5	0.15	25	0.5	0.0	30	1900	25000
SN2	5	0.15	30	0.7	0.0	30	1900	25000
SN3	5	0.05	25	0.5	0.0	30	1900	25000
SN4	5	0.3	25	0.5	0.0	30	1900	25000
SN5	5	0.15	30	0.5	0.0	30	1900	25000
SN6	5	0.15	35	0.5	0.0	30	1900	25000
SN7	5	0.15	25	0.7	0.0	30	1900	25000
SN8	5	0.15	35	0.7	0.0	30	1900	25000
SH1	5	0.15	25	0.5	0.0	60	2500	32600
SH2	5	0.3	35	0.7	0.0	60	2500	32600
IN1[(a)]	10	0.15	30	0.7	0.0	30	1900	25000
IN2	10	0.15	25	0.5	0.0	30	1900	25000
IN3	10	0.05	30	0.7	0.0	30	1900	25000
IN4	10	0.3	30	0.7	0.0	30	1900	25000
IN5	10	0.15	25	0.7	0.0	30	1900	25000
IN6	10	0.15	35	0.7	0.0	30	1900	25000
IN7	10	0.15	30	0.5	0.0	30	1900	25000
IN8	10	0.15	35	0.5	0.0	30	1900	25000
IH1	10	0.15	30	0.7	0.0	60	2500	32600
IH2	10	0.3	35	0.7	0.0	60	2500	32600
LN1	15	0.3	35	0.7	3.4	30	1900	25000
LN2	15	0.15	25	0.5	3.4	30	1900	25000
LN3	15	0.15	30	0.7	3.4	30	1900	25000
LH1[(a)]	15	0.3	35	0.7	3.4	60	2500	32600
LH2	15	0.3	25	0.5	3.4	60	2500	32600
LH3	15	0.05	35	0.7	3.4	60	2500	32600
LH4	15	0.15	35	0.7	3.4	60	2500	32600
LH5	15	0.3	25	0.7	3.4	60	2500	32600
LH6	15	0.3	30	0.7	3.4	60	2500	32600
LH7	15	0.3	35	0.5	3.4	60	2500	32600
LH8	15	0.3	30	0.5	3.4	60	2500	32600

[(a)] Reference column

6. Finite element analysis

Begum *et al*. (2007) developed a complete finite element model including the full cross-section and entire length of the column using the explicit module of the ABAQUS finite element code, which is used in the current study to assess the influence of important geometric and material parameters on the behaviour of PEC columns. The model is applicable for concentric as well as eccentric loads. The model components, along with the mesh configuration for a typical part between two consecutive links, are shown in Fig. 2. The steel plates were modelled using four-node shell elements. Eight-node brick elements were used for concrete, and beam elements for transverse links. A dynamic explicit solution strategy was implemented to trace a stable post-peak response in the load–deformation curve. The steel–concrete interface in the composite column was simulated using a contact pair algorithm. To represent the concrete material behaviour under partial confinement, the damage plasticity model in ABAQUS was implemented. The steel material properties are simulated with a trilinear elasto-plastic model including strain hardening.

Begum *et al*. (2007) used the developed model for PEC columns to reproduce the test results of 12 normal strength, seven high strength and two steel-fibre reinforced high strength concrete PEC columns. The average experimental-to-numerical ratios of the peak load obtained were: 1.01, 0.99 and 1.08, respectively, with standard deviations all less than 0.05. Moreover, the overall numerical load versus axial strain responses for the test columns were in very good agreement with the experimental responses. The failure in all the specimens observed in the numerical analyses was due to the initiation of local instability of the flange plate between two transverse links followed by crushing of the adjacent concrete. Similar behaviour was observed in the experiments. The full model also represented the axial capacity of the three long PEC test specimens ($L/d = 20$) with good accuracy, with an average experimental-to-numerical ratio of 0.98. Begum *et al* (2007) also studied the effect of local imperfections in the flanges and residual stresses in the steel plates of PEC columns on the axial capacity and failure behaviour of PEC columns. Since they found the

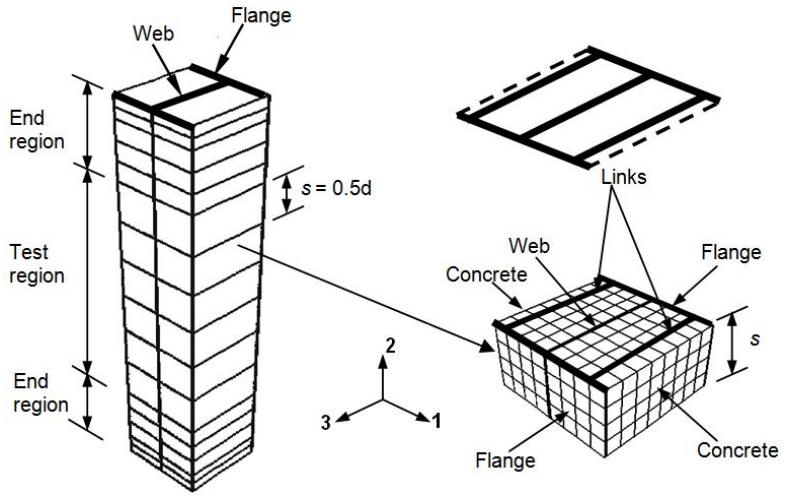

Fig. 2 Finite element mesh: (a) Typical PEC column displaying the parts between consecutive links; and (b) Mesh configuration of typical part in test region of column

effects of these two parameters on the behaviour of PEC columns to be negligible, in the FEM models of the parametric columns, local imperfections in the flanges and residual stresses in the steel plates were not included. However, global imperfections were included in the slender columns ($L/d = 15$) with a maximum amplitude of $L/2000 = 3.4$ mm, considered to be a typical value that is somewhat lower than the codified limit.

7. Results and discussion

This section presents the influence of each parameter on the behaviour of short, intermediate and long PEC columns in comparison to the three associated reference columns (i.e., SN1, IN1 and LH1, respectively) selected for the parametric study. The output parameters that have been extracted from the analysis results are: peak axial load, P_u, as well as moment, M_u, average axial strain, $\varepsilon_{a,u}$, and lateral displacement, $U_{3,u}$, all taken at the peak axial load. The term "moment" used in this paper always refers to the total bending moment (i.e., including the second-order effects) and is taken at mid-height of the column. The average axial strain is calculated by dividing the average total displacement in the axial direction by the length of the column. The axial load versus average axial strain, axial load versus lateral displacement, moment versus lateral displacement and axial load versus moment curves are also generated from the numerical analysis for each parametric column and are used in the following discussions on the influences of the variable parameters. The results obtained from the parametric analyses are organized and presented to highlight the individual effect of each parameter. To this end, the parametric columns that demonstrate the effect of a variable parameter for the three reference columns are divided into three sets: "Set 1", "Set 2" and "Set 3". "Set 1" includes the effect of the variable parameter on the short reference column, SN1, ($e/d = 0.15$, $b/t = 25$ and $s/d = 0.5$), "Set 2" demonstrates the effect on the intermediate-length reference column, IN1 ($e/d = 0.15$; $b/t = 30$; $s/d = 0.7$), and the effects of the variable parameter on the long reference column, LH1 ($e/d = 0.30$; $b/t = 35$; $s/d = 0.7$), are included in "Set 3".

The failure mode in each of the 31 parametric columns is studied using the numerical model. In general, the columns reached the peak load by concrete crushing either immediately preceded, immediately followed, or accompanied by local buckling of the flanges. The load level where the first sign of local buckling was observed is reported. This was done by plotting the axial load versus axial strain curves at the outside, inside and middle surfaces of the shell element of the flange plate where local buckling had taken place.

7.1 Effect of overall column slenderness ratio

7.1.1 Peak load and corresponding moment

Table 2 shows the effect of the overall column slenderness ratio (L/d) on the selected output parameters at the peak load point. For Set 1 and Set 2, the L/d ratio has the same effect on the ultimate axial load and moment. For these columns, increasing the L/d ratio from 5 to 10 reduces the ultimate axial load capacity by 3%, and increasing it to 15 results in an 8% reduction in the ultimate axial load. Although the actual strengths of the columns in Sets 1 and 2 are significantly different due to the local flange slenderness effects, the similarities in capacity reduction imply that for a moderate load eccentricity and normal strength concrete the global slenderness effects are essentially the same. The moments at the peak load points for both Sets 1 and 2 are increased

Table 2 Effect of overall column slenderness (L/d) ratio

Set	Column designation	Column properties					Magnitude of output parameters at peak load point				Percent difference		Occurrence of local buckling
		L/d	e/d	b/t	s/d	f_{cu} (MPa)	P_u (kN)	M_u (kN-m)	$\varepsilon_{a,u}$ ($\mu\varepsilon$)	$U_{3,u}$ (mm)	P_u (%)	M_u (%)	
	SN1[(a)]	**5**	0.15	25	0.5	30	6428	458	1382	3.7	—	—	after peak at $0.99P_u$
Set 1	IN2	**10**	0.15	25	0.5	30	6240	498	1213	12.3	-3	9	after peak at $0.97P_u$
	LN2	**15**	0.15	25	0.5	30	5922	601	1200	30.6	-8	31	after peak at $0.96P_u$
	SN2	**5**	0.15	30	0.7	30	5892	421	1370	3.9	—	—	at peak
Set 2	IN1[(a)]	**10**	0.15	30	0.7	30	5724	460	1202	12.9	-3	9	after peak at $0.99P_u$
	LN3	**15**	0.15	30	0.7	30	5410	551	1190	30.9	-8	31	after peak at $0.99P_u$
	SH2	**5**	0.30	35	0.7	60	6701	945	1184	6.0	—	—	after peak at $0.88P_u$
Set 3	IH2	**10**	0.30	35	0.7	60	6263	988	1008	22.8	-7	5	after peak at $0.91P_u$
	LH1[(a)]	**15**	0.30	35	0.7	60	5521	1036	904	49.3	-18	10	after peak at $0.92P_u$

(a) Reference column

by 9% and 31% for L/d ratios of 10 and 15, respectively, with respect to the moment for $L/d = 5$. The increase in the bending moment results from an increase in second-order moments as the column gets increasingly slender.

The effect of the L/d ratio observed in Set 3 is different from that observed in Sets 1 and 2. The ultimate load of column SH2 is reduced by 7% and 18%, respectively, for L/d of 10 and 15. These greater reductions are reflective of the increased influence of global slenderness when the eccentricity is larger and higher strength concrete is used. However, the moment at the peak load point is increased by only 5% and 10%, respectively, for L/d ratios of 10 and 15, with respect to that obtained for $L/d = 5$. This increase in the moment at the peak load point is significantly less than that observed for Sets 1 and 2 because the high load eccentricity ($e = 0.3d$) for columns included in Set 3 reduces the effect of the increase in the second-order displacements, as the L/d ratio increases, on the bending moment of these columns.

7.1.2 Load versus average axial strain response

Fig. 3 shows the effects of the L/d ratio on the axial load versus average axial strain responses. In Set 1 (Fig. 3(a)), column SN1 shows a flatter peak and more gradual post-peak strength decline as compared to columns IN2 ($L/d = 10$) and LN2 ($L/d = 15$). These three columns had e/d = 0.15, $b/t = 25$, $s/d = 0.5$ and were constructed with 30 MPa concrete. As shown in Fig. 3(b), for the Set 2 analyses, no significant difference is observed in the load versus strain response of columns IN1

and LN3. However, column SN2 shows ductile behaviour as compared to the other two. These columns had $e/d = 0.15$, $b/t = 30$, $s/d = 0.7$ and were constructed with 30 MPa concrete. In Fig. 3(c), no significant difference is observed in the load versus average axial strain curves of columns SH2, IH2 and LH1, except in the peak zone. All three columns show steep declines from the ultimate axial capacity.

Although the longer columns exhibit lower capacity and ductility in all sets, as expected, the effect on axial strength is far more pronounced for the columns with slender flange plates, larger load eccentricity, and higher strength concrete (i.e., Set 3). In some cases, significant differences in the failure mode are also revealed by changing the column slenderness. The clear benefit of the stockier flange plates (Set 1) on the failure mode of short columns diminishes as the columns become more slender. The difference in the brittleness of the failure mode as a function of column length is less distinct when the flange plates themselves are slender (Set 3), although this may have also been influenced by the different character of the higher concrete strength.

In the post-peak regions of the load versus strain responses, undulations are observed, particularly for the intermediate and long columns. As mentioned earlier, a dynamic solution strategy was implemented in the numerical simulations of the quasi-static response of PEC columns. After the peak load, the steel plate experiences local instability in several locations along the column length as the applied displacement increases. Moreover, as the column gets more slender, global instability becomes significant at higher levels of applied displacement. The instability in the steel plates causes the inertial forces to be significant, resulting in spurious oscillations in the residual portion of the load versus deformation responses.

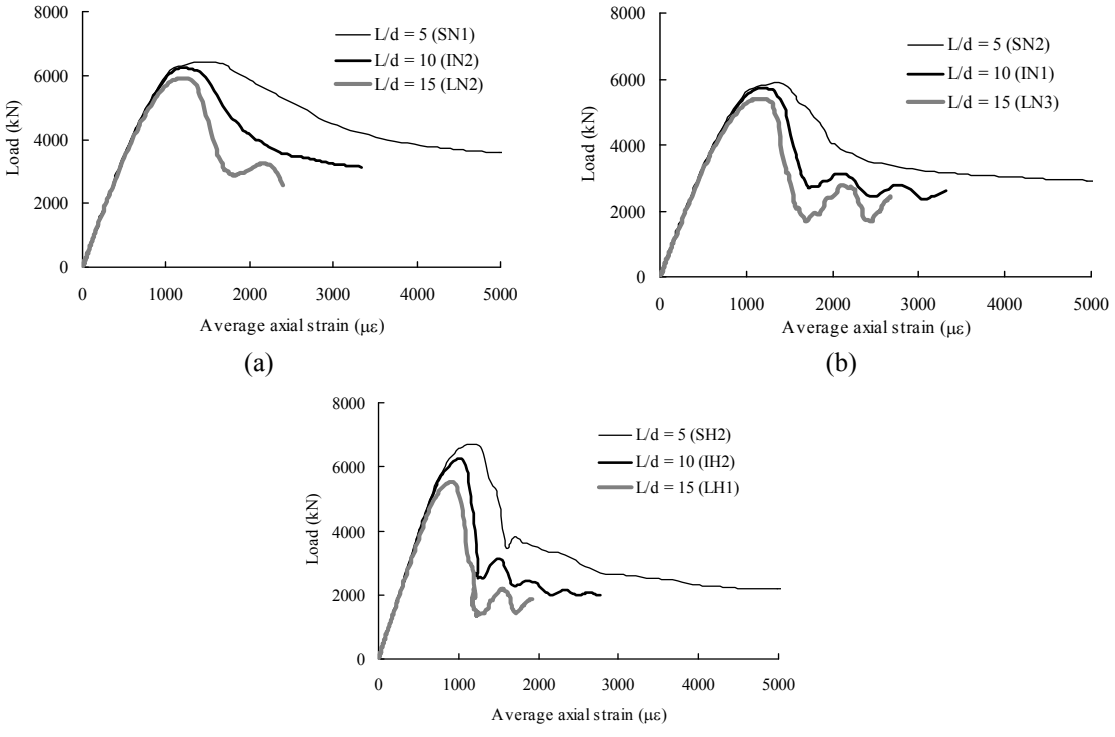

Fig. 3 Effect of L/d ratio on load versus average axial strain curve, (a) Set 1; (b) Set 2; and (c) Set 3

7.1.3 Load versus lateral displacement response

The effect of the L/d ratio on the load versus lateral displacement response is shown in Fig. 4. In all three sets, the pre-peak region of the load versus lateral displacement curves for the short columns (SN1, SN2 and SH2) show a steep slope and relatively linear behaviour. As the slenderness ratio (L/d) increases, this region of the curve becomes quite nonlinear with a significantly reduced initial slope. The nonlinear behaviour occurs due to the increased second-order displacement in the slender columns. The short columns experience a sharp decline in the post-peak region of the load versus lateral displacement curve, whereas the long columns can withstand the peak axial load over a wider range of lateral displacement.

In this case, the effect of increasing the slenderness ratio does not seem to be influenced greatly by the other parameters. All three sets show a much more rapid accumulation of lateral displacement as the global slenderness increases, although this accumulation is somewhat more pronounced in Set 3.

7.1.4 Load versus moment response

Fig. 5 presents the load versus moment curves for short, intermediate and long columns in each analysis set. In all three cases, the curves for the short columns represent essentially linear behaviour. However, as the L/d ratio increases, the curve shows nonlinear behaviour resulting from the effect of second-order displacements. The effect of global slenderness on the load versus moment curves is similar for the three sets, although the effect is somewhat less pronounced when the initial eccentricity is larger (Set 3) because the second-order displacement are, relative to the initial eccentricity, smaller.

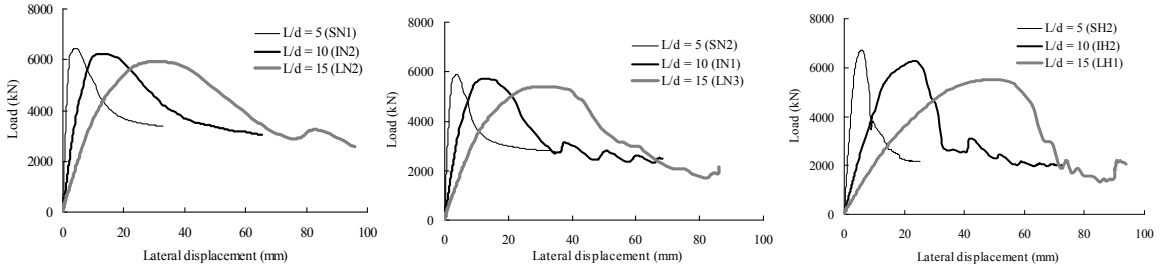

Fig. 4 Effect of L/d ratio on load versus lateral displacement curve, (a) Set 1; (b) Set 2; and (c) Set 3

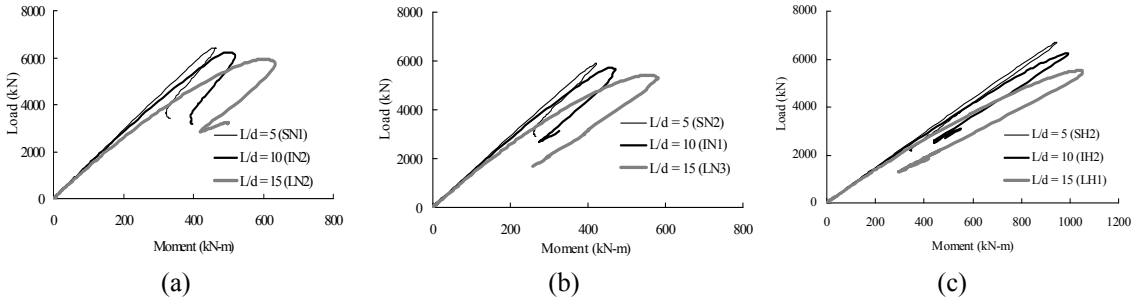

Fig. 5 Effect of L/d ratio on load versus moment curve, (a) Set 1; (b) Set 2; and (c) Set 3

7.1.5 Failure mode

The points of occurrence of local buckling in the reference columns (SN1, IN1 and LH1) for different L/d ratios are shown in Table 2. For column SN1 ($e/d = 0.15$, $b/t = 25$, $s/d = 0.5$), local buckling occurred shortly after the peak load. Increasing the L/d ratio is observed to delay the initiation of local buckling slightly.

The local buckling in column IN1 ($e/d = 0.15$, $b/t = 30$, $s/d = 0.7$) occurred after the crushing of concrete at 0.99 P_u. For this column, increasing the L/d ratio to 15 (column LN3) did not affect the failure mode. However, when the L/d ratio is reduced to 5 (i.e., column SN2), the local buckling was observed right at the peak load accompanied by concrete crushing.

On the other hand, for the long reference column LH1 ($e/d = 0.30$, $b/t = 35$, $s/d = 0.7$), local buckling occurred after the crushing of concrete at 0.92 P_u, and reducing the L/d ratio is observed to delay the local buckling somewhat. Although the long reference column, LH1, had the largest b/t ratio (i.e., 35) combined with the larger link spacing (i.e., 0.7d), it experienced local buckling well after the peak load. This column was constructed with high strength concrete and had a higher e/d ratio as compared to columns SN1 and IN1.

Table 3 Effect of load eccentricity (e/d) ratio

Set	Column designation	Column properties					Magnitude of output parameters at peak load point				Percent difference		Occurrence of local buckling
		L/d	e/d	b/t	s/d	f_{cu} (MPa)	P_u (kN)	M_u (kN-m)	$\varepsilon_{a,u}$ ($\mu\varepsilon$)	$U_{3,u}$ (mm)	P_u (%)	M_u (%)	
	SN3	5	0.05	25	0.5	30	7931	188	1547	1.2	—	—	after peak at $0.99P_u$
Set 1	SN1[(a)]	5	0.15	25	0.5	30	6428	458	1382	3.7	-19	144	after peak at $0.99P_u$
	SN4	5	0.30	25	0.5	30	4967	700	1334	5.8	-37	272	after peak at $0.99P_u$
	IN3	10	0.05	30	0.7	30	7268	195	1503	4.4	—	—	before peak at $0.97P_u$
Set 2	IN1[(a)]	10	0.15	30	0.7	30	5724	460	1202	12.9	-21	136	after peak at $0.99P_u$
	IN4	10	0.30	30	0.7	30	4287	678	1195	23.1	-41	247	after peak at $0.99P_u$
	LH3	15	0.05	35	0.7	60	10833	462	1546	16.8	—	—	before peak at $0.93P_u$
Set 3	LH4	15	0.15	35	0.7	60	8116	880	1288	37.6	-25	91	after peak at $0.97P_u$
	LH1[(a)]	15	0.30	35	0.7	60	5521	1036	904	49.3	-49	124	after peak at $0.92P_u$

(a) Reference column

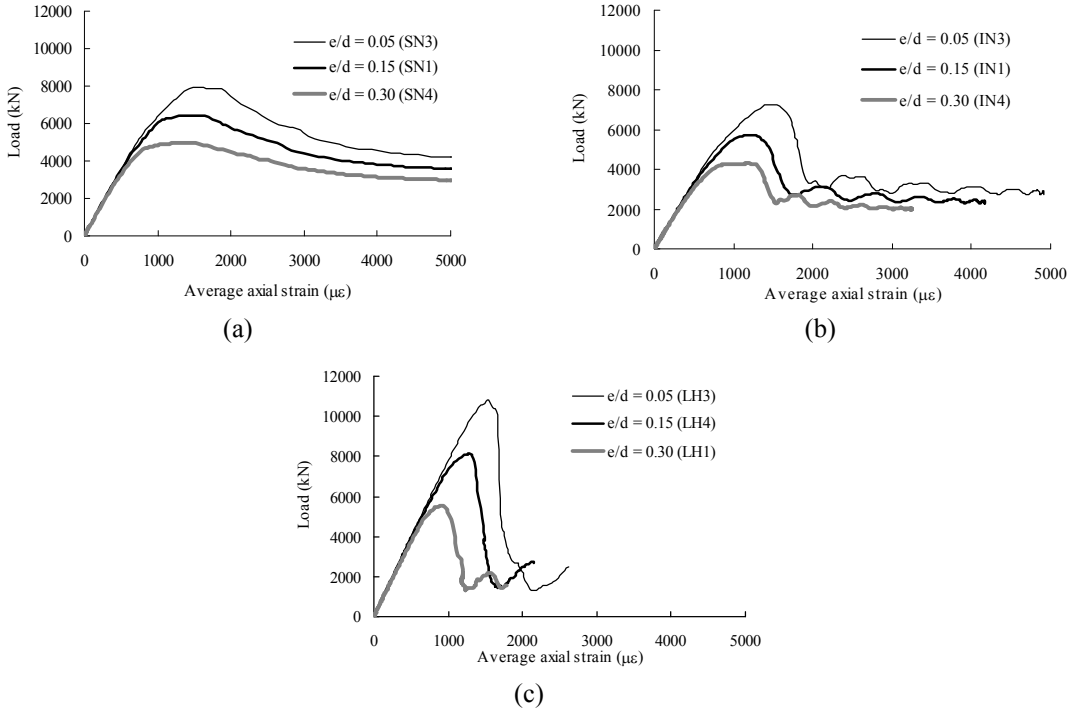

Fig. 6 Effect of *e*/*d* ratio on load versus average axial strain curve, (a) Set 1; (b) Set 2; and (c) Set 3

7.2 Effect of load eccentricity ratio

7.2.1 Peak load and corresponding moment

The influence of the load eccentricity ratio on the axial load capacity of the PEC columns is observed to be significant (see Table 3). For both Sets 1 and 2, the peak loads corresponding to $e/d = 0.05$ are reduced by approximately 20% and 40% when the e/d ratio is increased to 0.15 and 0.30, respectively, implying that the effects of increasing load eccentricity on the capacity of short and intermediate PEC columns are not greatly affected by the flange slenderness or link spacing in the range examined. For Set 3, with greater flange slenderness and higher concrete strength, the reductions in capacity are even greater, with decreases of 25% and 49% for $e/d = 0.15$ and 0.30, respectively.

As observed in Table 3, for both Set 1 and Set 2 the average value of the increase in the moment corresponding to the peak load is about 140% and 260% for e/d ratio of 0.15 and 0.30, respectively. For Set 3, however, the increase in moment was observed to be significantly lower: 90% and 124%, respectively, for $e/d = 0.15$ and 0.30. This is primarily due to the reduced sensitivity of the ultimate second-order effects in slender columns to the initial load eccentricity.

7.2.2 Load versus average axial strain response

Fig. 6 shows the effect of the load eccentricity ratio on the axial load versus average axial strain curve for the three sets of analyses. No difference is observed in the initial portion of the load–strain behaviour within each set. However, the variation in the e/d ratio affects the peak and post-peak region of the load versus average axial strain response. In Sets 1 and 2, a flatter peak

followed by a slightly more gradual post-peak strength decline is observed as the *e*/*d* ratio increases. On the other hand, all three columns in Set 3 experienced a sharp decline in the post-peak region, indicating a negligible effect of the increased bending moment (resulting from the increase in the *e*/*d* ratio) on the level of brittleness in the behaviour of these columns. Conversely, the axial strain at the peak is significantly affected in Set 3; a 17% and 42% reduction in the average axial strain at the peak load is observed by increasing the *e*/*d* ratio from 0.05 to 0.15 and 0.30, respectively.

The effect of increased initial load eccentricity on the axial capacity and corresponding axial strain is more pronounced as the column becomes more slender. The brittle failure mode of the long reference column (which was constructed with high strength concrete and slender plates) is not affected at all by the *e*/*d* ratio. The capacities of the short and intermediate reference columns are reduced by 20% on an average, but with a better post-peak response, as the *e*/*d* ratio increases. These columns were constructed with normal strength concrete and had variations in plate slenderness and link spacing.

7.2.3 Load versus lateral displacement and moment versus lateral displacement responses

The effects of the load eccentricity ratio on the load versus lateral displacement response are presented in Fig. 7. In all three sets, the lateral displacement at a particular load increases with an increase in the *e*/*d* ratio, as expected. The increase in lateral displacement is more pronounced in the cases of intermediate and long columns (Figs. 7(b) and 7(c)) due to the lower flexural stiffness of the column. These figures also show that the peak region of the curve becomes relatively flat with a gradual drop in axial load capacity in the descending branch as the *e*/*d* ratio increases.

As shown in Fig. 8, the moment at the column mid-height increases significantly with the increase in the *e*/*d* ratio in all three sets due to the significant differences in the load eccentricity. The lateral displacement at the peak moment also increases with increasing *e*/*d* ratio, but this effect is far more evident in the long columns (Set 3) due to the more influential second-order deflection. However, the moment versus lateral displacement curves for long columns (with high strength concrete) show a sharper decline in the descending branch as compared to the short (Set 1) and intermediate (Set 2) PEC columns.

7.2.4 Failure mode

For Set 1 that includes the short columns, the occurrence of local buckling is not affected by the

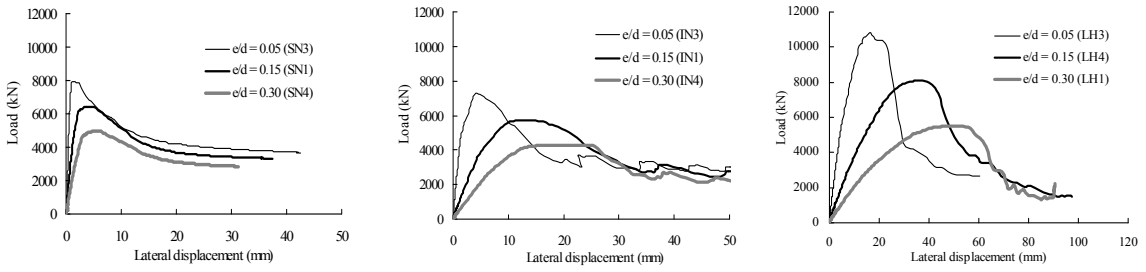

(a) (b) (c)

Fig. 7 Effect of *e*/*d* ratio on load versus lateral displacement curve, (a) Set 1; (b) Set 2; and (c) Set 3

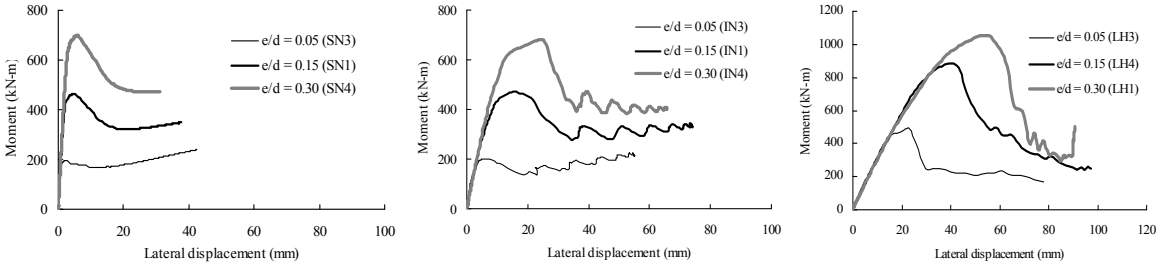

Fig. 8 Effect of *e*/*d* ratio on moment versus lateral displacement curve, (a) Set 1; (b) Set 2; and (c) Set 3

load eccentricity ratio, as shown in Table 3. For all three values of load eccentricity ratio, the short columns experienced local buckling shortly after the peak at an axial load of $0.99P_u$. In the case of the intermediate reference column IN1, reducing the load eccentricity accelerates the occurrence of local buckling, which is observed in column IN3. On the other hand, when the load eccentricity ratio is increased to 0.30 (column IN4) no change is observed in the load corresponding to the first sign of local buckling.

In Set 3, the long reference column LH1 also experiences local buckling earlier as the *e*/*d* ratio reduces to 0.15 and 0.05, in comparison with that observed with *e*/*d* = 0.30. Among all the long columns analysed for the parametric study, only column LH3 experienced local buckling well before reaching the peak load. This long column was also the only one loaded at *e*/*d* = 0.05, which indicates the presence of higher axial compression and lower bending moment as compared to the columns with higher *e*/*d* ratios.

7.3 Effect of flange plate slenderness ratio and link spacing-to-depth ratio

7.3.1 Peak load and corresponding moment

In Table 4, for Set 1 and Set 2, nearly identical changes are observed for the peak load and corresponding moment when the *b*/*t* ratio is changed from 25 to 30 and 35 for each s/d ratio. For long columns, which are included in Set 3, the reductions in the peak load and moment due to the increase in *b*/*t* ratio are slightly lower than those observed in Set 1 and Set 2.

Increasing the *b*/*t* ratio from 25 to 30 causes a 6% to 8% reduction in the axial load capacity of the PEC columns in all three sets for the two link spacings. The average reduction in axial capacity is 7.5%. The *L*/*d* ratio and concrete strength seemed to have little or no effect on the reduction in axial capacity due to the increase in plate slenderness. The average reduction in capacity for *b*/*t* = 35 is 13%, ranging from 11% (long columns) to 16% (short columns).

The average reduction in the moment corresponding to the peak axial load is 7% and 13% respectively, for *b*/*t* ratios of 30 and 35, with respect to the moment for *b*/*t* = 25. The minimum reduction was observed in long columns, i.e., 5% for *b*/*t* = 30 and 10% for *b*/*t* = 35. On the other hand, the maximum reduction was observed for short columns, i.e., 8% for *b*/*t* = 30 and 17% for *b*/*t* = 35. The variations in the link spacing seemed to have a negligible influence on these results.

Table 4 Effect of flange plate slenderness (b/t) ratio with different s/d ratios

Set	Column designation	Column properties					Magnitude of output parameters at peak load point				Percent difference		Occurrence of local buckling
		L/d	e/d	b/t	s/d	f_{cu} (MPa)	P_u (kN)	M_u (kN-m)	$\varepsilon_{a,u}$ ($\mu\varepsilon$)	$U_{3,u}$ (mm)	P_u (%)	M_u (%)	
Set 1	SN1[(a)]	5	0.15	**25**	0.5	30	6428	458	1382	3.7	—	—	after peak at $0.99P_u$
	SN5	5	0.15	**30**	0.5	30	5917	422	1371	3.8	-8	-8	after peak at $0.99P_u$
	SN6	5	0.15	**35**	0.5	30	5548	395	1361	3.9	-14	-14	after peak at $0.99P_u$
	SN7	5	0.15	**25**	0.7	30	6406	456	1383	3.7	—	—	after peak at $0.99P_u$
	SN2	5	0.15	**30**	0.7	30	5892	421	1370	3.9	-8	-8	at peak
	SN8	5	0.15	**35**	0.7	30	5411	380	1119	2.7	-16	-17	before peak at $0.99P_u$
Set 2	IN2	10	0.15	**25**	0.5	30	6240	498	1213	12.3	—	—	after peak at $0.97P_u$
	IN7	10	0.15	**30**	0.5	30	5743	462	1203	12.9	-8	-7	after peak at $0.98P_u$
	IN8	10	0.15	**35**	0.5	30	5384	435	1193	13.3	-14	-13	after peak at $0.98P_u$
	IN5	10	0.15	**25**	0.7	30	6224	497	1214	12.4	—	—	after peak at $0.98P_u$
	IN1[(a)]	10	0.15	**30**	0.7	30	5724	460	1202	12.9	-8	-7	after peak at $0.99P_u$
	IN6	10	0.15	**35**	0.7	30	5327	420	1100	11.4	-14	-15	before peak at $0.99P_u$
Set 3	LH2	15	0.30	**25**	0.5	60	6200	1154	971	47.7	—	—	after peak at $0.88P_u$
	LH8	15	0.30	**30**	0.5	60	5814	1098	958	50.5	-6	-5	after peak at $0.88P_u$
	LH7	15	0.30	**35**	0.5	60	5548	1041	904	49.3	-11	-10	after peak at $0.92P_u$
	LH5	15	0.30	**25**	0.7	60	6200	1147	959	46.6	—	—	after peak at $0.87P_u$
	LH6	15	0.30	**30**	0.7	60	5797	1082	929	48.2	-7	-6	after peak at $0.87P_u$
	LH1[(a)]	15	0.30	**35**	0.7	60	5521	1036	904	49.3	-11	-10	after peak at $0.92P_u$

(a) Reference column

7.3.2 Load versus average axial strain response

Figs. 9, 10 and 11 present the effects of the plate slenderness, b/t, on the load versus average axial strain curves for short, intermediate and long columns, respectively, with two different link spacings. In all cases, as expected, the peak load decreases as the slenderness of the flange plate increases. In addition, in the cases of short and intermediate columns, as the b/t ratio increases the

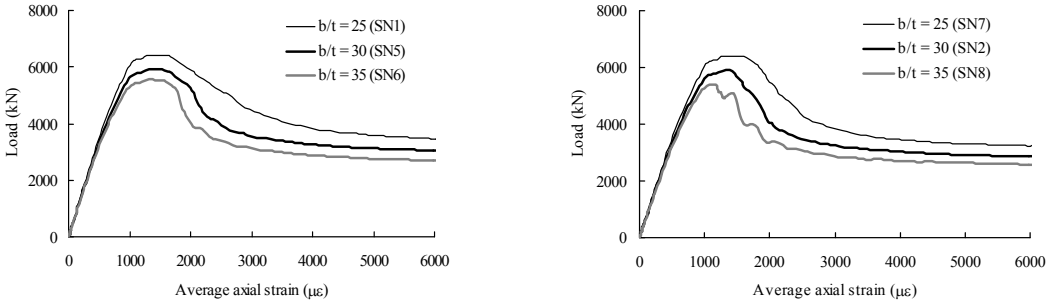

(a) (b)

Fig. 9 Effect of b/t ratio on load versus average axial strain response for short PEC columns (Set 1), (a) $s = 0.5d$; and (b) $s = 0.7d$

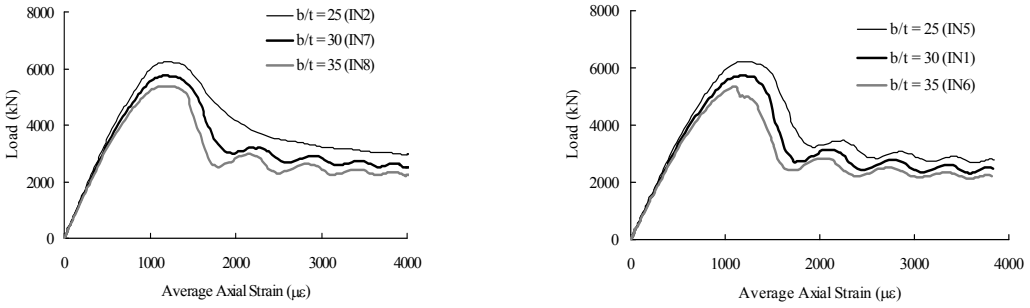

(a) (b)

Fig. 10 Effect of b/t ratio on load versus average axial strain response for intermediate PEC columns (Set 2), (a) $s = 0.5d$; and (b) $s = 0.7d$

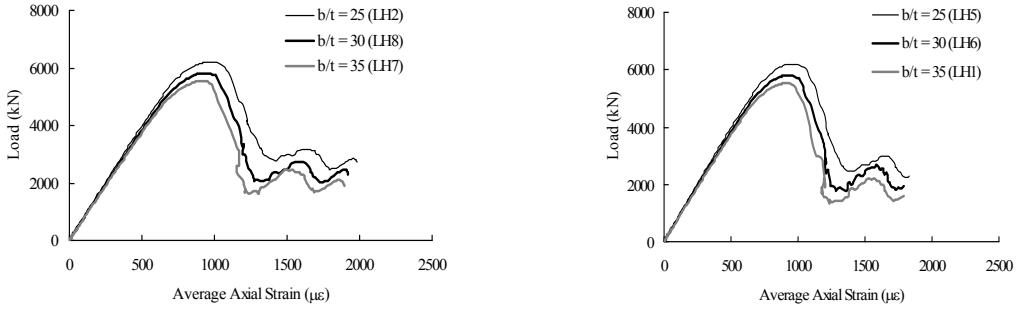

(a) (b)

Fig. 11 Effect of b/t ratio on load versus average axial strain response for long PEC columns (Set 3), (a) $s = 0.5d$; and (b) $s = 0.7d$

responses of the columns become slightly less ductile as indicated by the descending branches of the curves. However, in the case of the slender columns, the flange plate slenderness ratio seemed to have a diminished effect on the load versus average axial strain curve. This can be attributed in part to the fact that in these slender columns, local buckling in the steel flanges occurred after the ultimate load point. Therefore, as the column becomes slender, the advantage of using a stockier flange plate diminishes for both values of s/d ratio (0.5 and 0.7).

7.3.3 Failure mode

As shown in Table 4, for three different values of b/t ratio (i.e., 25, 30 and 35) including the short reference column (SN1), for which $e/d = 0.15$ and $s/d = 0.5$, local flange buckling occurred at the same load level ($0.99P_u$) after reaching the peak load. When the same column is fabricated with links spaced at $0.7d$, increasing the plate b/t ratio from 25 to 35 accelerated the occurrence of local buckling in the flanges very slightly. In column SN7, with $b/t = 25$ and $s/d = 0.7$, local buckling is observed at $0.99P_u$ after the crushing of concrete at the peak load. The same column when fabricated with plates having b/t ratios of 30 (column SN2) and 35 (column SN8), local buckling occurred with and slightly before the crushing of concrete, respectively.

In the case of intermediate columns (included in Set 2) with links spaced at $0.5d$ and plate b/t ratios of 25, 30 and 35, designated as IN2, IN7 and IN8, respectively, local buckling took place shortly after the peak axial load. The plate slenderness ratio is observed to have no significant effect on the failure modes of these columns. However, among the intermediate columns with a $0.7d$ link spacing, column IN6, with $b/t = 35$, showed local buckling before the peak load, whereas columns IN5 ($b/t = 25$) and IN1 ($b/t = 30$) experienced local buckling after reaching the peak load.

None of the long columns (Set 3) experienced local buckling before reaching the peak load, as shown in Table 4. Columns LH7 and LH1, which had the most slender flange plates ($b/t = 35$), experienced local buckling slightly earlier as compared to the columns with $b/t = 25$ and 30. In general, buckling of the flange tends to occur earlier as it becomes more slender and the effect of the b/t ratio on local buckling is more prominent for the link spacing $s = 0.7d$. The chance of the occurrence of local buckling before the peak load, as the plate gets increasingly slender, reduces with increased L/d ratios.

7.4 Effect of concrete compressive strength

7.4.1 Peak load and corresponding moment

The effect of normal and high strength concrete with nominal strengths of 30 and 60 MPa, respectively, is studied in Table 5. The ultimate axial load of column SN1 ($e/d = 0.15$, $b/t = 25$, $s/d = 0.5$), IN1 ($e/d = 0.15$, $b/t = 30$, s/d = 0.7) and LN1 ($e/d = 0.30$, $b/t = 35$, $s/d = 0.7$), which were constructed with 30 MPa concrete, are increased by 57%, 60% and 48%, respectively, when 60 MPa concrete is used instead. (For reference, the increases in capacity based on a pure cross-sectional analysis under concentric axial load for b/t ratios of 25, 30 and 35 would be 48%, 53% and 58%, respectively.) This indicates that the benefits of using higher strength concrete become significantly discounted as local and global instability increase in influence. The moment at the peak load is also increased by 55% for columns SN1 and LN1 and 69% for column IN1. The average increase in the peak load and corresponding moment for all three columns with different e/d, b/t and s/d ratios are 55% and 57%, respectively.

Table 5 Effect of concrete compressive strength

Set	Column designation	Column properties					Magnitude of output parameters at peak load point				Percent difference		Occurrence of local buckling
		L/d	e/d	b/t	s/d	f_{cu} (MPa)	P_u (kN)	M_u (kN-m)	$\varepsilon_{a,u}$ ($\mu\varepsilon$)	$U_{3,u}$ (mm)	P_u (%)	M_u (%)	
Set 1	SN1[(a)]	5	0.15	25	0.5	**30**	6428	458	1382	3.7	—	—	after peak at $0.99P_u$
	SH1	5	0.15	25	0.5	**60**	10100	712	1538	2.9	57	55	after peak at $0.89P_u$
Set 2	IN1[(a)]	10	0.15	30	0.7	**30**	5724	460	1202	12.9	—	—	after peak at $0.99P_u$
	IH1	10	0.15	30	0.7	**60**	9160	776	1430	17.3	60	69	after peak at $0.94P_u$
Set 3	LN1	15	0.3	35	0.7	**30**	3736	667	926	40.2	—	—	after peak at $0.92P_u$
	LH1[(a)]	15	0.3	35	0.7	**60**	5521	1036	904	49.3	48	55	after peak at $0.92P_u$

(a) Reference column

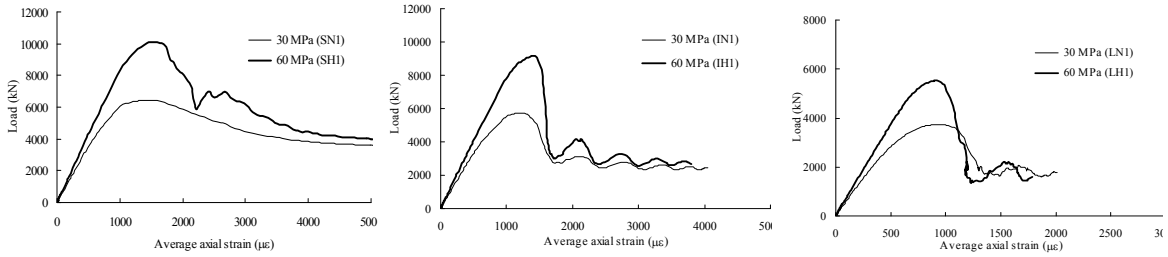

(a) (b) (c)

Fig. 12 Effect of concrete compressive strength on load versus average axial strain curve, (a) Set 1; (b) Set 2; and (c) Set 3

7.4.2 Load versus average axial strain

As expected, the behaviour of the PEC columns is greatly affected by the compressive strength of concrete for all three sets of analysis, as shown in Fig. 12. The axial load versus average strain response for PEC columns with high strength concrete show steeper slopes in the initial portions of the curves due to the higher modulus of elasticity of the concrete. Columns SH1, IH1 and LH1 (60 MPa concrete) also demonstrate sharp post-peak strength declines as compared to colums SN1, IN1 and LN1 (30 MPa concrete), respectively. However, for the long columns (LN1 and LH1) the level of brittleness was somewhat less affected by the concrete strength because the brittle failures of the long columns are primarily due to the effect of increased bending moment resulting from increased lateral displacements.

7.4.3 Failure mode

The local flange buckling in column SN1 ($e/d = 0.15$, $b/t = 25$, $s/d = 0.5$) and IN1 ($e/d = 0.15$, $b/t = 30$, $s/d = 0.7$) occurred shortly after the crushing of concrete at a load of $0.99P_u$, as indicated in Table 5. When high strength concrete is used in these columns—columns SH1 and IH1—local buckling is observed to be delayed. The loads corresponding to the first sign of local buckling in the flanges were $0.89P_u$ and $0.94P_u$, respectively, for columns SH1 and IH1. However, the concrete compressive strength did not affect initiation of local buckling in the flanges of the long column (LH1), since the long column behaviour is governed by global bending. Both of the long columns (LN1 and LH1), which had $e/d = 0.30$, $b/t = 35$ and $s/d = 0.7$, experienced local buckling at $0.92P_u$ after reaching the peak axial load.

8. Conclusions

A comprehensive parametric analysis was performed to study the behaviour of PEC columns subjected to axial compression and bending about the strong axis. Four geometric and one material parameter were varied and their influences were demonstrated with respect to the peak axial load and corresponding moment, failure mode and overall column load–deformation responses. The important findings of the study presented in this chapter are as follows:

- The axial capacity of a PEC column reduces as the overall slenderness ratio increases, particularly for columns with slender plates. The ductility of a normal strength concrete column reduces as the column becomes slender. However, the level of brittleness at failure for high strength concrete PEC columns is not affected significantly by the overall column slenderness.
- The presence of a higher bending moment (resulting from a high e/d ratio) reduces the column capacity significantly. The occurrence of local buckling is also affected by the e/d ratio. The columns with lower e/d ratios experienced local flange buckling before, or very shortly after, the peak load.
- As the flange plate slenderness ratio increases, the axial capacity of the column reduces, as expected, with increased brittleness in the failure behaviour. These effects are more prominent in short columns with a larger link spacing. On the other hand, the brittle behaviour of long PEC columns is not affected significantly by the b/t ratio. Thus, the advantage of using stockier flange plates diminishes as the column becomes slender.
- The axial capacity of a PEC column, with a variety of L/d, e/d, b/t and s/d ratios, is greatly improved (average increase is 55%) by the use of high strength (60 MPa) concrete instead of normal strength (30 MPa) concrete. However, the load–deformation response of high strength concrete PEC columns indicated brittle failure as compared to columns with normal strength concrete.

References

ACI (1992) ACI Committee 363. State-of-the-Art Report on High-Strength Concrete, ACI 363R-92, Farmington Hills, MI, USA, pp.1-55.

Almusallam, T.H. and Alsayed, S.H. (1995), "Stress–Strain Relationship of Normal, High Strength and Lightweight concrete", *Mag. Concrete Res.*, **47**(170), 39-44.

Begum, M., Driver, R.G. and Elwi, A.E. (2007), "Finite element modeling of partially encased composite columns using the dynamic explicit solution method", *J. Struct. Eng., ASCE*, **133**(3), 326-334.

Bouchereau, R. and Toupin, J.-D. (2003), "Étude du Comportement en Compression-Flexion des Poteaux Mixtes Partiellement Enrobés", Report EPM/GCS-2003-03; Department of Civil, Geological and Mining Engineering, Ecole Polytechnique, Montreal, Canada.

Chen, Y., Wang, T., Yang, J. and Zhao, X. (2010), "Test and numerical simulation of partially encased composite columns subject to axial and cyclic horizontal loads", *Int. J. Steel Struct.*, **10**(4), 385-393.

Chicoine, T., Tremblay, R. and Massicotte, B. (2002), "Finite element modelling and design of partially encased composite columns", *Steel Compos. Struct., Int. J.*, **2**(3), 171-194.

Chicoine, T., Massicotte, B. and Tremblay, R. (2003), "Long-term behavior and strength of partially-encased composite columns with built up shapes", *J. Struct. Eng., ASCE*, **129**(2), 141-150.

Correia, A.J.P.M. and Rodrigues, J.P.C. (2011), "Fire resistance of partially encased steel columns with restrained thermal elongation", *J. Construct. Steel Res.*, **67**(4), 593-601.

CSA (2009), Design of Steel Structures, CSA S16-09; Canadian Standards Association, Mississauga, ON, Canada.

Dastfan, M. and Driver, R.G. (2010a), "Large scale test of a modular steel plate shear wall with PEC columns", *Proceedings of the 9th US National and 10th Canadian Conference on Earthquake Engineering*, Toronto, ON, Canada, July.

Dastfan, M. and Driver, R.G. (2010b), "Large scale test of a steel plate shear wall with PEC columns and RBS connections", *Proceedings of Annual Stability Conference*, Structural Stability Research Council, Orlando, FL, USA, May.

Deng, X., Dastfan, M. and Driver, R.G. (2008), "Behaviour of steel plate shear walls with composite columns", *Proceedings of American Society of Civil Engineers Structures Congress*, Vancouver, BC, Canada, April.

Prickett, B.S. and Driver, R.G. (2006), "Behaviour of partially encased composite columns made with high performance concrete", Structural Engineering Report No 262; Department of Civil and Environmental Engineering, University of Alberta, AB, Canada.

Rashid, M.A., Mansur, M.A. and Paramasivum, P. (2002), "Correlation between mechanical properties of high strength concrete", *J. Mater. Civil Eng., ASCE*, **14**(3), 230-238.

Tremblay, R., Massicotte, B., Filion, I. and Maranda, R. (1998), "Experimental study on the behaviour of partially encased composite columns made with light welded *h*-steel shapes under compressive axial loads", *Proceedings of SSRC Annual Technical Session & Meeting*, Atlanta, GA, USA, September, pp. 195-204.

Uy, B. (2001), "Local and postlocal buckling of fabricated steel and composite cross sections", *J. Struct. Eng.*, **127**(6), 666-677.

Young, B. and Ellobody, E. (2011), "Performance of axially restrained concrete encased steel composite columns at elevated temperatures", *Eng. Struct. J.*, **33**(1), 245-254.

Zhao, G. and Feng, C. (2012), "Axial ultimate capacity of partially encased composite columns", *Appl. Mech. Mater.*, **166-169**, 292-295.

BU

List of Symbols

b/t	Width-to-thickness ratio of flange plate
B	Unsupported flange width
D	Depth of column cross-section
E	Initial load eccentricity
e/d	Initial load eccentricity ratio
E_c	Modulus of elasticity for concrete (secant modulus at $0.45f_{cu}$)
E_s	Modulus of elasticity for steel
f_{cu}	Uniaxial compressive strength of concrete
F_s	Yield strength of steel plate
L	Column Length
L/d	Overall column slenderness ratio
P_u	Peak axial load
M_u	Moment at peak axial load
S	Link spacing
s/d	Link spacing-to-depth ratio
T	Plate thickness
$U_{3,u}$	Lateral displacement at peak axial load
$\varepsilon_{a,u}$	Average axial strainat peak axial load
ε_{cu}	Axial strain of concrete at f_{cu}
ε_y	Yield strain of steel